Inorganic Chemistry
Article

Inorg. Chem. **2009**, *48*, 11865–11870 **11865**
DOI: 10.1021/ic902046t

Photochemical Activation of an Azido Manganese-Monosubstituted Keggin Polyoxometalate: On the Road to a Mn(V)−Nitrido Derivative

G. Izzet,[†,‡] E. Ishow,[‡] J. Delaire,[‡] C. Afonso,[§] J.-C. Tabet,[§] and A. Proust*[,†,∥]

[†]*Institut Parisien de Chimie Moléculaire, UMR CNRS 7201, Equipe Polyoxométallates Case courier 42, UPMC Univ Paris 06, 4 place Jussieu, 75252 Paris cedex 05, France,* [‡]*Laboratoire de Photophysique et Photochimie Moléculaire, ENS Cachan, UMR CNRS 8531, 61 avenue du Président Wilson 94235 Cachan, France,* [§]*Institut Parisien de Chimie Moléculaire, UMR CNRS 7201, Equipe Spectrométrie de masse, UPMC Univ Paris 06, 4 place Jussieu, 75252 Paris cedex 05, France, and* [∥]*Institut Universitaire de France, 75005 Paris, France*

Received October 15, 2009

The manganese(V)−nitrido polyoxometalate derivative $[PW_{11}O_{39}\{Mn^{V}N\}]^{5-}$ has been synthesized by photochemical activation of the parent manganese(III)−azido derivative $[PW_{11}O_{39}Mn^{III}N_3]^{5-}$. It was characterized by mass spectrometry, ^{31}P NMR, UV−vis, and IR spectroscopies. An electrochemistry study indicated that only the Mn(V) state was stable. The photoactivation of the manganese(III)−azido derivative proceeds through two competitive routes, yielding to the targeted product of photooxidation $\{Mn^{V}N\}$ or the undesirable product of photoreduction $\{Mn^{II}L\}$ (L = H_2O, N_3), depending on the photolysis conditions. A simplified photolysis mechanism involving two different excited states was proposed to account for the temperature and wavelength dependence.

Introduction

Polyoxometalates (POMs) are a class of well-defined oxo nanoclusters with a diversity of structures and properties.[1−3] They have found numerous applications in analytical chemistry, catalysis, materials science, or medicine. In particular, many Keggin-type polyanions, incorporating one or several transition metals, have been studied for their catalytic activity in oxygenation reactions.[4−7] Their thermal stability as well as their robustness under oxidative conditions have been put forward.[8−11] The ability of such transition-metal-substituted POMs to transfer an oxygen atom has been well established. We recently turned our attention toward the synthesis of nitrido derivatives and their ability to transfer a nitrogen atom.

Our first approach to synthesize such complexes was based on the insertion of a preformed metal−nitrido function on a lacunary POM, typically $[PW_{11}O_{39}]^{7-}$. Such a methodology allowed us to synthesize Cr^{V}, Ru^{VI}, Re^{VI}, and Os^{VI} POM-based nitrido complexes.[12−16] Unfortunately, it could not be extended to manganese complexes. The reaction of ammonia in the presence of an oxidant[17] is an alternative synthetic path to nitrido derivatives[18−22] but can hardly be considered here because of the intrinsic instability of POMs in basic media.

*To whom correspondence should be addressed. E-mail: anna.proust@upmc.fr.

(1) Pope, M. T. *Heteropoly and Isopoly Oxometalates*; Springer-Verlag: New York, 1983; Vol. *8*.
(2) Pope, M. T. In *Comprehensive Coordination Chemistry II*; McCleverty, J., Meyer, T. J., Eds.; Elsevier: Oxford, 2004; Vol. *4*, pp 635−678.
(3) Hill, C. L. *Chem. Rev.* **1998**, *98*, 1−390 (special issue devoted to polyoxometalates).
(4) Hill, C. L.; Brown, R. B. *J. Am. Chem. Soc.* **1986**, *108*, 536–538.
(5) Hill, C. L.; Prosser McCartha, C. M. *Coord. Chem. Rev.* **1995**, *143*, 407–455.
(6) Neumann, R. *Prog. Inorg. Chem.* **1998**, *47*, 317−370.
(7) Mizuno, N.; Yamaguchi, K.; Kamata, K. *Coord. Chem. Rev.* **2005**, *249*, 1944–1956.
(8) Geletii, Y. V.; Botar, B.; Koegerler, P.; Hillesheim, D. A.; Musaev, D. G.; Hill, C. L. *Angew. Chem., Int. Ed.* **2008**, *47*, 3896–3899.
(9) Sartorel, A.; Carraro, M.; Scorrano, G.; De Zorzi, R.; Geremia, S.; McDaniel, N. D.; Bernhard, S.; Bonchio, M. *J. Am. Chem. Soc.* **2008**, *130*, 5006–5007.
(10) Geletii, Y. V.; Huang, Z. Q.; Hou, Y.; Musaev, D. G.; Lian, T. Q.; Hill, C. L. *J. Am. Chem. Soc.* **2009**, *131*, 7522–7523.
(11) Kuznetsov, A. E.; Geletii, Y. V.; Hill, C. L.; Morokuma, K.; Musaev, D. G. *J. Am. Chem. Soc.* **2009**, *131*, 6844–6854.
(12) Kwen, H.; Tomlinson, S.; Maatta, E. A.; Dablemont, C.; Thouvenot, R.; Proust, A.; Gouzerh, P. *Chem. Commun.* **2002**, 2970–2971.
(13) Dablemont, C.; Hamaker, C. G.; Thouvenot, R.; Sojka, Z.; Che, M.; Maatta, E. A.; Proust, A. *Chem.—Eur. J.* **2006**, *12*, 9150–9160.
(14) Lahootun, V.; Besson, C.; Villanneau, R.; Villain, F.; Chamoreau, L. M.; Boubekeur, K.; Blanchard, S.; Thouvenot, R.; Proust, A. *J. Am. Chem. Soc.* **2007**, *129*, 7127–7135.
(15) Lahootun, V.; Karcher, J.; Courillon, C.; Launay, F.; Mijares, K.; Maatta, E.; Proust, A. *Eur. J. Inorg. Chem.* **2008**, 4899–4905.
(16) Besson, C.; Musaev, D. G.; Lahootun, V.; Cao, R.; Chamoreau, L. M.; Villanneau, R.; Villain, F.; Thouvenot., R.; Geletii, Y.; Hill, C. L.; Proust, A. *Chem.—Eur. J.* **2009**, *15*, 10233–10243.
(17) Dehnicke, K.; Strahle, J. *Angew. Chem., Int. Ed. Engl.* **1992**, *31*, 955–978.
(18) Hill, C. L.; Hollander, F. J. *J. Am. Chem. Soc.* **1982**, *104*, 7318–7319.
(19) Du Bois, J.; Tomooka, C. S.; Hong, J.; Carreira, E. M. *Acc. Chem. Res.* **1997**, *30*, 364–372.

Published on Web 11/24/2009

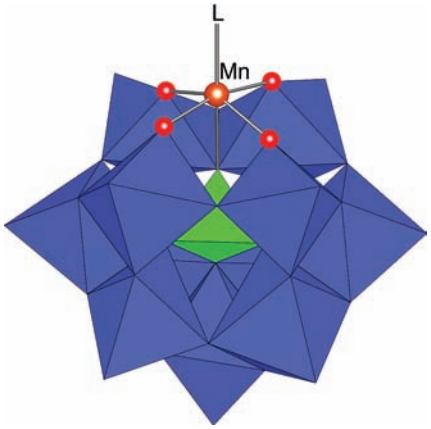

Figure 1. Schematic polyhedric representation of anion $[PW_{11}O_{39}Mn(L)]^{n-}$.

Another path consists of intermetallic transfer.[23−25] It has been successfully applied to the synthesis of manganese−nitrido complexes of multidentate ligands, including corroles,[26−28] but has failed in our hands, up to now. Finally, a last path to nitrido derivatives relies on photoactivation of azido complexes,[29] which has largely been described in the case of manganese.[30,31] Since reported examples of *N*-atom transfer to an organic substrate from isolated metal−nitrido complexes are restricted to ruthenium[32,33] and manganese,[20,34−38] this drove us to investigate the synthesis of a Mn^V POM-based nitrido complex. We thus describe here the synthesis and photoactivation of $[PW_{11}O_{39}Mn^{III}(N_3)]^{5-}$ (Figure 1), as a *n*-tetrabutylammonium (TBA) salt, and the characterization of $[PW_{11}O_{39}\{Mn^VN\}]^{5-}$ as a photoproduct. The photoactivation of the $\{Mn^{III}N_3\}$ function is known to proceed through two competitive routes, yielding respectively the targeted product of photooxidation $\{Mn^VN\}$ or the undesirable product of photoreduction $\{Mn^{II}L\}$ (L = H_2O, N_3). Therefore, influence of the experimental conditions, especially the choice of the wavelength, will also be discussed.

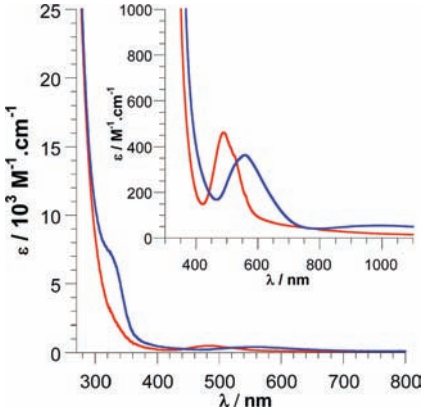

Figure 2. Room-temperature electronic spectra of **TBA-2(OH$_2$)** (red) and **TBA-2(N$_3$)** (blue) in CH_3CN.

Results: Formation and Characterization of $[PW_{11}O_{39}\{MnN\}]^{5-}$ (3). Synthesis and Characterization of $(TBA)_5[PW_{11}O_{39}Mn^{III}(N_3)]$. Starting compounds $K_5[PW_{11}O_{39}Mn^{II}(OH_2)]$ (**K-1(OH$_2$)**) and $K_4[PW_{11}O_{39}Mn^{III}(OH_2)]$ (**K-2(OH$_2$)**) were obtained according to the reported methods.[39−41] The conversion to a tetrabutyl ammonium salt involved a metathetical exchange by the addition of a slight excess of TBABr (4.2 equiv) to an aqueous solution of an alkali salt of the polyoxometalate. This reaction resulted in the immediate precipitation of $(TBA)_4[PW_{11}O_{39}Mn^{III}(OH_2)]$ (**TBA-2(OH$_2$)**) as a pink solid in a fairly good yield, which was successively washed with water, ethanol, and diethyl ether. Its purity was ascertained by elemental analysis. The addition of an excess of $TBAN_3$ to a solution of **TBA-2(OH$_2$)** in acetonitrile led to an immediate color change from pink to purple. Compound **TBA-2(N$_3$)** was then precipitated with diethyl ether and quickly washed with ethanol. The IR absorption spectrum of **TBA-2(N$_3$)** displays an intense antisymmetric stretch, $\nu_{as}(N_3)$ at 2046 cm^{-1}. Its UV−vis absorption spectrum in CH_3CN is dominated by the O → W ligand-to-metal charge transfer (LMCT) of the polyoxometalate centered at 260 nm. The shoulder localized around 335 nm is compatible with the charge-transfer band N_3 → Mn and the $\pi\pi^*$ transition of the coordinated azide ligand (Figure 2). Lowering the temperature transforms the shoulder into a peak but, unfortunately, does not allow distinguishing of the contribution of the LMCT from $\pi\pi^*$ transition (see the figure in the Supporting Information). Finally, the bands at 559 and 990 nm are attributed to d−d transitions centered on the Mn(III).[42]

Cyclic voltammograms of **TBA-2(OH$_2$)** and **TBA-2(N$_3$)** were recorded. Two well-defined quasi-reversible and nonreversible waves are observed with $E_{1/2}$ = −0.10 V/SCE (ΔE = 260 mV) and $E_{1/2}$ = −1.69 V/SCE (ΔE = 80 mV) for **TBA-2(OH$_2$)** and $E_{1/2}$ = −0.16 V/SCE (ΔE = 480 mV) and $E_{1/2}$ = −1.74 V/SCE (ΔE = 100 mV) for **TBA-2(N$_3$)** corresponding to the Mn^{III}/Mn^{II} couple and

(20) Minakata, S.; Ando, T.; Nishimura, M.; Ryu, I.; Komatsu, M. *Angew. Chem., Int. Ed.* **1998**, *37*, 3392–3394.
(21) Chang, C. J.; Connick, W. B.; Low, D. W.; Day, M. W.; Gray, H. B. *Inorg. Chem.* **1998**, *37*, 3107–3110.
(22) Lam, W. W. Y.; Man, W. L.; Leung, C. F.; Wong, C. Y.; Lau, T. C. *J. Am. Chem. Soc.* **2007**, *129*, 13646–13652.
(23) Neely, F. L.; Bottomley, L. A. *Inorg. Chem.* **1997**, *36*, 5432–5434.
(24) Chang, C. J.; Low, D. W.; Gray, H. B. *Inorg. Chem.* **1997**, *36*, 270–271.
(25) Woo, L. K. *Chem. Rev.* **1993**, *93*, 1125–1136.
(26) Birk, T.; Bendix, J. *Inorg. Chem.* **2003**, *42*, 7608–7615.
(27) Golubkov, G.; Gross, Z. *J. Am. Chem. Soc.* **2005**, *127*, 3258–3259.
(28) Golubkov, G.; Goldberg, I.; Bendix, J.; Gross, Z. *J. Inorg. Biochem.* **2001**, *86*, 236–236.
(29) Sima, J. *Coord. Chem. Rev.* **2006**, *250*, 2325–2334.
(30) Groves, J. T.; Takahashi, T. *J. Am. Chem. Soc.* **1983**, *105*, 2073–2074.
(31) Meyer, K.; Bendix, J.; Metzler-Nolte, N.; Weyhermuller, T.; Wieghardt, K. *J. Am. Chem. Soc.* **1998**, *120*, 7260–7270.
(32) Leung, S. K. Y.; Huang, J. S.; Liang, J. L.; Che, C. M.; Zhou, Z. Y. *Angew. Chem., Int. Ed.* **2003**, *42*, 340–343.
(33) Man, W. L.; Lam, W. W. Y.; Yiu, S. M.; Lau, T. C.; Peng, S. M. *J. Am. Chem. Soc.* **2004**, *126*, 15336–15337.
(34) Bottomley, L. A.; Neely, F. L. *J. Am. Chem. Soc.* **1988**, *110*, 6748–6752.
(35) Ho, C. M.; Lau, T. C.; Kwong, H. L.; T., W. W. *J. Chem. Soc., Dalton Trans.* **1999**, 2411–2414.
(36) Nishimura, M.; Minakata, S.; Thongchant, S.; Ryu, I.; Komatsu, M. *Tetrahedron Lett.* **2000**, *41*, 7089–7092.
(37) Yiu, S. M.; Lam, W. W. Y.; Ho, C. M.; Lau, T. C. *J. Am. Chem. Soc.* **2007**, *129*, 803–809.
(38) Eikey, R. A.; Abu-Omar, M. M. *Coord. Chem. Rev.* **2003**, *243*, 83–124.
(39) Tourné, C. M.; Tourné, G. F.; Malik, S. A.; Weakley, T. J. R. *J. Inorg. Nucl. Chem.* **1970**, *32*, 3875–3890.
(40) Katsoulis, D. E.; Pope, M. T. *J. Chem. Soc., Dalton Trans.* **1989**, 1483–1489.
(41) Zhang, X. Y.; Pope, M. T.; Chance, M. R.; Jameson, G. B. *Polyhedron* **1995**, *14*, 1381–1392.
(42) Lever, A. B. P. *Inorganic Electronic Spectroscopy*; 2nd ed.; Elesevier: Amsterdam, 1984.

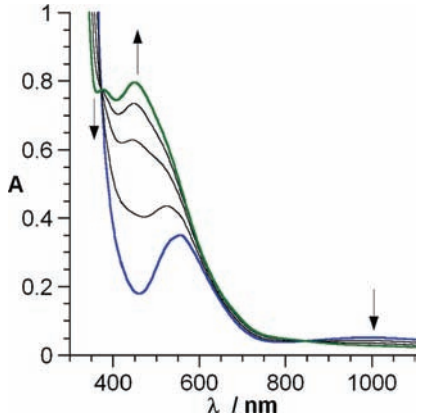

Figure 3. Spectral changes observed during the photolysis of **TBA-2(N_3)** (1 mM) in a CH_3CN solution at −30 °C with λ_{exc} = 313 nm (P = 14.5 mW).

to a one-electron reduction of the tungstic framework, respectively.

Photolysis of TBA-2(N_3), Formation of TBA-3. Photolysis (λ_{exc} = 313 nm) of a solution of **TBA-2(N_3)**, obtained by mixing **TBA-2(OH_2)** with an excess of $TBAN_3$ (4 equiv), in anhydrous acetonitrile was performed at −30 °C with a Hg/Xe lamp source equipped with an appropriate bandpass filter. [An excess of $TBAN_3$ is essential to ensure the full conversion to **TBA-3**. Otherwise, a mixture with the starting materials is observed, due to the equilibrium between **TBA-2(N_3)** and **TBA-2(OH_2)** in solution and competitive decomposition of free $TBAN_3$ under the photolysis conditions.] Figure 3 shows the spectral changes observed as a function of time. During irradiation, the intense CT band of **TBA-2(N_3)** at 335 nm and the d−d transition at 990 nm decrease while new bands at 379 and 449 nm appear. Two isosbestic points at ∼375 and 845 nm are observed. After 1 h of irradiation (P = 14.5 mW) of a solution of **TBA-2(N_3)** (3 mL, 1 mM), the absorbance of the solution does not evolve any more, which attests the completion of the photolysis.

The photoproduct slowly decomposes within a few days, as can be optically attested to by bleaching of the originally brownish solution. The ^{31}P NMR spectrum of a freshly prepared solution exhibits only one sharp signal due to a diamagnetic species at −11.9 ppm that we attributed to $(TBA)_5[PW_{11}O_{39}\{Mn^VN\}]$ (**TBA-3**). Its integration is similar to that of an authentic sample of $(TBA)_3[PW_{12}O_{40}]$ (δ = 14.1 ppm), at the same concentration as that of the initial solution of **TBA-2(N_3)**. This demonstrates that the reaction is quantitative and that paramagnetic species, affording ^{31}P NMR signals sometimes too broad to be detected (like **TBA-2(N_3)**), are negligible, if present at all. In the same way, a freshly photolyzed solution of **TBA-2(N_3)** is EPR-silent, which attests to the absence of Mn^{II} species as photoreduction products. The formation of a nitrido species is also supported by its IR spectrum (see the figure in the Supporting Information), recorded as a KBr pellet, which displays a new weak band at 1023 cm^{-1} consistent with a Mn≡N triple bond. Photolysis of **TBA-2(N_3)** at 313 nm and low temperatures thus yields the corresponding Mn^V−nitrido derivative as a second example of a Mn^V-containing POM.[43]

The electrospray ionization (ESI) mass spectrum of the photolyzed solution displays two main isotopic clusters centered at m/z 687 (91%) and at m/z 997 (100%) assigned to $[HPW_{11}O_{39}\{Mn^VN\}]^{4-}$ and $\{(TBA)[HPW_{11}O_{39}\{Mn^VN\}]\}^{3-}$ aggregates, respectively (Figure 4). Minor isotopic clusters centered at m/z 697 (16%), m/z 917 (7.5%), m/z 1077 (8.9%), and m/z 1616 (15%) assigned to $[KPW_{11}O_{39}\{Mn^VN\}]^{4-}$, $[H_2PW_{11}O_{39}\{Mn^VN\}]^{3-}$, $\{(TBA_2)[PW_{11}O_{39}\{Mn^VN\}]\}^{3-}$, and $\{(TBA_2)[HPW_{11}O_{39}\{Mn^VN\}\}^{2-}$ aggregates, respectively, are also observed. Each isotopic cluster presents a slight contribution (∼25%) of the parent $[PW_{11}O_{39}Mn^{III}]^{4-}$ (insets in Figure 4) due to the decomposition of the nitrido complex in the solution (as otherwise observed).[34] The declustering conditions have a great impact on the nitrido complex's relative abundance, as displayed in Figure 4b. After one week, only the decomposed species could be evidenced from same solution (data not shown).

A cyclic voltammogram of **TBA-3** is depicted in Figure 5. Two monoelectronic irreversible processes and a monoelectronic quasi-reversible wave are observed with Ep_{ox} = 0.44 V/SCE, Ep_{red} = −1.44 V/SCE, and $E_{1/2}$ = −1.81 V/SCE (ΔE = 100 mV) corresponding respectively to Mn^{VI}≡N/Mn^V≡N and Mn^V≡N/Mn^{IV}≡N couples and a one-electron reduction of the tungstic framework. The small waves observed around 0 V/SCE corresponding to the previously described Mn^{III}/Mn^{II} couple are due to decomposition of the instable Mn^{VI}≡N and Mn^{IV}≡N complexes, once formed. The cyclic voltammetry thus nicely demonstrated that no Mn^{II}- or Mn^{III}-containing compounds, neither **1** nor **2**, were initially present in the solution after photolysis.

All of these data suggest that photooxidation of **TBA-2(N_3)** prevails under these conditions according to eq 1.

$$(TBA)_5[PW_{11}O_{39}Mn^{III}(N_3)] \xrightarrow{h\nu} (TBA)_5[PW_{11}O_{39}\{Mn^VN\}] + N_2 \quad (1)$$

The above photooxidation is quantitative, as assessed by ^{31}P NMR, cyclic voltammetry, and IR according to the disappearance of the $\nu(N_3)$ stretch.

Influence of the Experimental Photolysis Conditions (Wavelength and Temperature). When the photolysis is carried out at room temperature, the UV−vis spectrum of the solution after completion of the reaction is slightly less intense than when performed at −30 °C. In the same way, increasing the excitation wavelength of the photolysis (335 and 365 nm) produces less colored solutions, suggesting an increasing presence of the colorless photoreduction product **TBA-1(OH_2/N_3)** (Figure 6) due to homolytic cleavage of the Mn^{III}−N_3 bond and generation of a $N_3^\bullet$ radical which decomposes to dinitrogen (eq 2). The formation of the photoreduction product was ascertained by EPR and IR spectrocopies by comparison with authentic samples of **TBA-1(OH_2)** and **TBA-1(N_3)**.

$$(TBA)_5[PW_{11}O_{39}Mn^{III}(N_3)] \xrightarrow{h\nu} (TBA)_5[PW_{11}O_{39}Mn^{II}] + \frac{3}{2}N_2 \quad (2)$$

(43) Khenkin, A. M.; Kumar, D.; Shaik, S.; Neumann, R. *J. Am. Chem. Soc.* **2006**, *128*, 15451–15460.

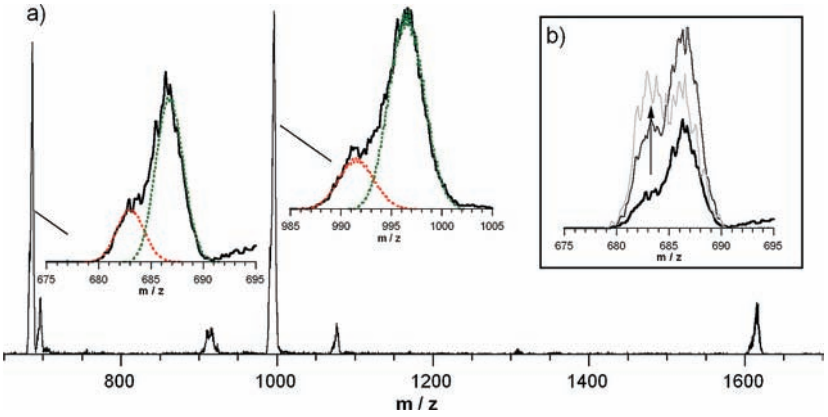

Figure 4. (a) ESI spectra of a 10 pmol L^{-1} CH_3CN solution of **TBA-3** recorded using the negative ion mode. Inset: Enlargement of the base peaks of the $[HPW_{11}O_{39}\{Mn^{V}N\}]^{4-}$ aggregate (left) and the $\{(TBA)[HPW_{11}O_{39}\{Mn^{V}N\}]\}^{3-}$ aggregate (right). The simulated spectra of $[HPW_{11}O_{39}\{Mn^{V}N\}]^{4-}$ and $\{(TBA)[HPW_{11}O_{39}\{Mn^{V}N\}]\}^{3-}$ aggregates are represented in green dotted lines, while the simulated spectra of $[PW_{11}O_{39}Mn^{III}]^{4-}$ and $\{(TBA)[PW_{11}O_{39}Mn^{III}]\}^{3-}$ are represented in red dotted lines. (b) Evolution of the m/z 683 ($[PW_{11}O_{39}Mn^{III}]^{4-}$) and m/z 687 ($[HPW_{11}O_{39}\{Mn^{V}N\}]^{4-}$) species as a function of the declustering potential is represented: soft (25 V, black bold), mild (70 V, dark gray), harsh (120 V, pale gray).

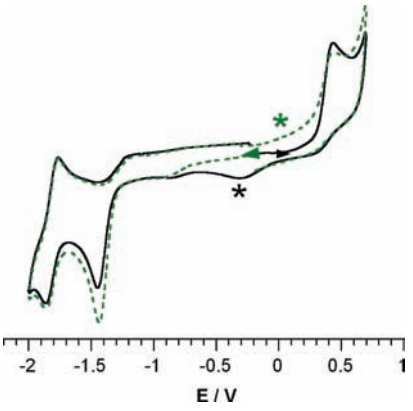

Figure 5. Cyclic voltammograms of **TBA-3** (10^{-3} M) in CH_3CN with 10^{-1} M $TBABF_4$ as a supporting electrolyte. The waves noted with a star correspond to the Mn^{III}/Mn^{II} couple of **TBA-2(N_3)** or **TBA-2(OH_2)** formed by decomposition of $Mn^{VI}{\equiv}N$ (black solid line) and $Mn^{IV}{\equiv}N$ (green dotted line) complexes. The waves starting at −0.8 and 0.6 V/SCE correspond to the reduction of traces of O_2 and the oxidation of N_3^- in excess, respectively.

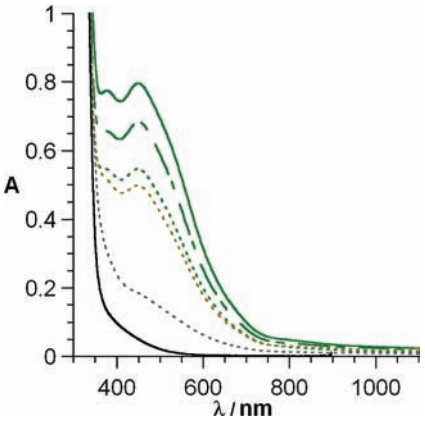

Figure 6. UV−vis−near IR absorption spectra of solutions of **TBA-2(N_3)** (1 mM) in CH_3CN after photolysis under different experimental conditions. λ_{exc} = 313 nm, T = −30 °C (solid green line); λ_{exc} = 313 nm, T = −10 °C (dashed green line); λ_{exc} = 313 nm, T = 25 °C (dotted green line); λ_{exc} = 335 nm, T = 25 °C (dotted kaki line); λ_{exc} = 365 nm, T = 25 °C (dotted gray line). **TBA-1(N_3)** (1 mM) in CH_3CN (solid black line). In each case, irradiation times were chosen until the end of the photolytic reaction.

The set intensity of the lamp during the photolysis had no effect on the UV−vis absorption spectrum of the solution at the end of the reaction. This attests to the fact that the observed difference of the photoproducts distribution clearly comes from a dependence on the excitation wavelength energy. The absorption at 449 nm allowed us to quantify the formation of the photooxidation versus photoreduction products depending on the experimental conditions of the photolysis (Table 1), since the starting **TBA-2(N_3)** was fully converted according to the disappearance of its IR $\nu(N_3)$ stretch. We therefore conclude that the best conditions of forming the targeted nitrido compound are high energy excitation (λ_{exc} = 313 nm) and low temperature. Nevertheless, low-temperature photolysis (−30 °C) with a low energy excitation (λ_{exc} = 365 nm) also produces mainly the photooxidation product, albeit at a dramatically slower rate.

Discussion: Photooxidation versus Photoreduction

Very few studies reporting the photolysis of azido−metal complexes are exceedingly focused on the competition between the photooxidation and the photoreduction reactions. In one case, a simple four-state model was proposed to account for the different reactivity of iron−azido complexes as a function of the spin state of the metal center.[44] Furthermore, photolysis temperature has already been found to be a very critical experimental parameter governing the product distribution.[31,44−46] In these examples, photooxidation was observed when the photolysis was performed in a frozen solution, while only photoreduction occurred in a liquid solution. The authors proposed that the reduced mobility of the azide radical in a frozen solution makes the photoreduction pathway partially reversible, thus increasing the observable yield of the photooxidation pathway. In the same way, encapsulation of salen metal−azido complexes into zeolite allowed their photooxidation, while no photoreaction

(44) Song, Y. F.; Berry, J. F.; Bill, E.; Bothe, E.; Weyhermuller, T.; Wieghardt, K. *Inorg. Chem.* **2007**, *46*, 2208–2219.
(45) Meyer, K.; Bill, E.; Mienert, B.; Weyhermuller, T.; Wieghardt, K. *J. Am. Chem. Soc.* **1999**, *121*, 4859–4876.
(46) Grapperhaus, C. A.; Mienert, B.; Bill, E.; Weyhermuller, T.; Wieghardt, K. *Inorg. Chem.* **2000**, *39*, 5306–5317.

Table 1. Photooxidation and Photoreduction under Different Photolysis Conditions

photolysis conditions[a]	photooxidation conversion (%)	photoreduction conversion (%)
λ_{exc} = 313, nm T = −30 °C	100	0
λ_{exc} = 313, nm T = −10 °C	85	15
λ_{exc} = 313, nm T = 25 °C	66	34
λ_{exc} = 335, nm T = 25 °C	60	40
λ_{exc} = 365, nm T = 25 °C	18	82

[a] Bandpass filter with ±5 nm.

was observed when the complexes were present in solution.[47] To the best of our knowledge, the wavelength dependence of the nature of the photoproducts during photolysis of a metal−azido complex was only reported once.[31] In this example, when the photolysis of a manganese−azido complex was performed under UV irradiation (185 and 254 nm), only a photoreduction product was formed (independently of the photolysis temperature,) while photooxidation prevailed when the photolysis was performed at −35 °C with ∼350 nm light.

In our case, the photolysis excitation wavelength λ_{exc} has a major effect on the distribution of the photoproducts. At room temperature, the photooxidation versus photoreduction conversion ratio is 1.94 for λ_{exc} = 313 nm, while it is 0.22 for λ_{exc} = 365 nm. The fact that the ratio drops by an order of magnitude when changing the excitation wavelength in a 50 nm range strongly suggests that at least two different close energy excited states are involved in the photooxidation and photoreduction reactions. A simple five-states model is proposed to account for the different reactivity as a function of the wavelength excitation and the temperature of the photolysis. These states are shown as the energy curves in Figure 7. When the photolysis is performed with high-energy excitation (313−335 nm), the major photoproduct is the Mn^{V}−nitrido derivative (green bold curve). The excited state implied must contain a $\pi\pi^*$ character (green thin curve) and decomposes with the release of N_2, possibly through adiabatic crossing from the azide excited-state surface to the nitrido-excited surface (not represented in Figure 7), as proposed by Formentín et al. for the photoactivation of salen azido−metal complexes.[47] When the photolysis is performed with a lower-energy excitation wavelength (365 nm), the major product is the Mn^{II} complex (black bold curve). The excited state implied must then contain a charge transfer $N_3 \rightarrow$ Mn character (black thin curve) and decomposes by homolytic cleavage of the Mn−N_3 bond. Finally, as only photooxidation prevails when the photolysis is performed at low temperatures (−30 °C), whatever the excitation wavelength applied (from 313 to 365 nm), we can assume that the reaction that has the highest activation barrier is the homolytic cleavage of the Mn−N_3 bond (represented as a bold arrow in Figure 7).

Compound **TBA-2(N_3)** thus displays a very unusual reactivity during its photolysis. In fact, since in most molecules the vibration levels of the electronic excited states lie close together and because internal conversion (IC) between electronic state neighboring energies is very fast, molecules in higher states quickly reach the lowest electronic excited state.

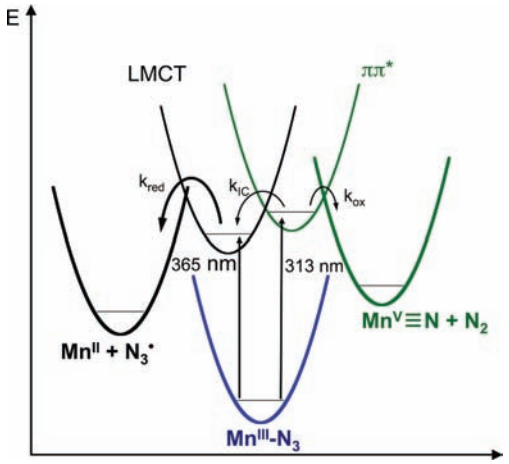

Figure 7. Proposed simplified photolysis mechanism described by a five-states model.

This observation is referred to as Vavilov-Kasha's rule.[48,49] Exceptions to this rule are found in media where other relaxation channels successfully compete with IC. Such an anomaly is observed in azulene molecules,[49] in which IC is relatively slow. In larger systems like polymers or molecular crystals, where the IC rate is high, deviations from Vavilov-Kasha's rule are due more to ultrafast decay into states other than the lowest fluorescent state.[50] The Vavilov-Kasha rule was reformulated by Demas and Crosby for transition metal complexes:[51] *in the absence of photochemistry from upper excited states, emission will occur from the lowest electronic excited state* (*general case*) *or from those states that can achieve a significant Boltzmann population relative to the lowest excited state*. In the present study, a reasonable explanation to the apparent violation to the Vavilov-Kasha rule would be that the kinetic constant (k_{ox}) of the Mn^{V}−nitrido formation from the higher-energy excited state $\pi\pi^*$ would have the same order of magnitude as the IC (k_{IC}) toward the near MLCT state. On the other hand, as only photooxidation prevails at low temperatures, we can conclude that k_{red}, the rate constant of the Mn^{II} formation, is much smaller than k_{ox}.

Summary and Conclusion

We have presented here the synthesis and full characterization of $(TBA)_5[PW_{11}O_{39}\{MnN\}]$. This complex was quantitatively synthesized by photochemical activation of the corresponding manganese(III)−azido complex. We found that the nature of the photoproducts strongly depends on the photolysis conditions, temperature, and wavelength. To explain this, a simplified photolysis mechanism involving two different excited states was proposed. We are currently exploring the reactivity of the manganese(V) nitrido complex which is expected to be highly active for nitrogen transfer.

Our approach provides the first application of the azide activation route to the synthesis of nitrido derivatives of polyoxometalates. Furthermore, it opens the route to catalytical *N*-transfer since photoconversion of metal azido into metal−nitrido derivatives could be involved in a catalytic cycle.

(47) Formentín, P.; Folgado, J. V.; Fornés, V.; García, H.; Márquez, F.; Sabater, M. J. *J. Phys. Chem. B* **2000**, *104*, 8361–8365.
(48) Kasha, M. *Faraday Soc. Discuss.* **1950**, 14–19.
(49) Birks, J. B. *Photophysics of Aromatic Molecules*; Wiley: London, 1970.
(50) Frolov, S. V.; Bao, Z. *Phys. Rev. Lett.* **2000**, *85*, 2196–2199.
(51) Demas, J. N.; Crosby, G. A. *J. Am. Chem. Soc.* **1970**, *92*, 7262–7270.

Experimental Section

Synthesis. Reagent-grade solvents and reagents were purchased and used as received, unless otherwise stated. Acetonitrile was distilled from calcium hydride under argon. Tetrabutylammonium tetrafluoroborate was synthesized from commercial (Aldrich) sodium tetrafluoroborate and tetrabutylammonium hydrogen sulfate. The reagents $K_7[PW_{11}O_{39}]\cdot 14H_2O$,[52] $K_4[PW_{11}O_{39}Mn^{III}(OH_2)]$ (**K-2(OH$_2$)**),[39−41] and tetrabutylammonium azide[53] were synthesized according to the published procedures. [Hygroscopic solid tetrabutylammonium azide was gently heated under a vacuum to desiccate it. The temperature must be cautiously controlled and kept strictly below 50 °C to avoid the formation and concentration of explosive byproducts.] Chemical analyses were performed by the Service de Microanalyses (Université Pierre et Marie Curie, Paris, France) and the Laboratoire Central d'Analyses du CNRS (Vernaison, France).

Preparation of (TBA)$_5$[PW$_{11}$O$_{39}$Mn^{II}(OH$_2$)], TBA-1(OH$_2$). To a solution of $K_7PW_{11}O_{39}$ (3.0 g, 0.937 mmol) in distilled water (3 mL) was added $MnCl_2\cdot 4H_2O$ (0.204 g, 1.03 mmol). The colorless solution instantly turned orange. It was stirred for 10 min. A solution of CsCl (1.7 g, 10.1 mmol) in a minimum amount of distilled water was then added to the solution, which immediately precipitated. It was filtrated, washed with a EtOH/H_2O (1/1) mixture, and redissolved in a 0.1 M AcOH/AcOLi (1/1) buffer (50 mL). TBABr (1.5 g, 4.66 mmol) was added to the solution that instantly precipitated. It was filtrated, washed with distilled water, and redissolved in MeCN precipitated by the addition of ether to yield **TBA-1(OH$_2$)** as a colorless solid (3.0 g, 81%). IR (KBr) ν_{max} (cm^{-1}): 377 (s) 402 (w), 515 (w), 593 (w), 725 (w), 817 (vs), 889 (s), 955 (s), 1057 (s), 1153 (w), 1381 (w), 1484 (m), 2875 (m), 2939 (m), 2962 (m).

Preparation of (TBA)$_4$[PW$_{11}$O$_{39}$Mn^{III}(OH$_2$)], TBA-2(OH$_2$). To a solution of **K-2(OH$_2$)** (0.936 g, 0.322 mmol) in distilled water (10 mL) was added TBABr (0.436 g, 1.35 mmol). The TBA salt of **2(OH$_2$)** precipitated immediately. It was filtrated and washed until the supernatant became colorless. The solid was then washed with ethanol and diethyl ether to give **TBA-2(OH$_2$)** as a pink solid (0.750 mg, 63%). Anal. Calcd for $C_{64}H_{146}MnN_4O_{40}PW_{11}$: C, 20.66; H, 3.96; Mn, 1.48; N, 1.51; O, 17.20; P, 0.83; W, 54.36. Found: C, 20.54; H, 3.87; N, 1.55; P, 0.91; W, 52.6. IR (KBr) ν_{max} (cm^{-1}): 386 (m), 518 (w), 596 (w), 626 (w), 805 (vs), 882 (s), 962 (s), 1074 (s), 1086 (m), 1153 (w), 1381 (w), 1484 (m), 2874 (m), 2935 (m), 2962 (m). UV−vis (CH_3CN): 260 nm (42500 M^{-1} cm^{-1}), 490 (460 M^{-1} cm^{-1}).

Preparation of (TBA)$_5$[PW$_{11}$O$_{39}$Mn^{III}(N$_3$)], TBA-2(N$_3$). To a solution of **TBA-2(OH$_2$)** (0.160 g, 0.043 mmol) in distilled MeCN (5 mL) was added an excess of $(Bu_4N)N_3$ (0.04 g, 0.141 mmol). The pink solution turned instantaneously purple. Compound **TBA-2(N$_3$)** was precipitated by addition of diethyl ether. It was filtrated and quickly washed with ethanol to give **TBA-2(N$_3$)** as a purple solid. Anal. Calcd for $C_{80}H_{180}MnN_8O_{39}PW_{11}$: C, 24.10; H, 4.55; N, 2.81. Found: C, 23,75; H, 4.47; N, 2.71. IR (KBr) ν_{max} (cm^{-1}): 385 (s), 391 (s), 502 (w), 518 (m), 596 (w), 634 (w), 687 (w), 807 (vs), 880 (s), 958 (s), 1069 (s), 1091 (m), 1153 (w), 1382 (w), 1485 (m), 2046 (s), 2875 (m), 2937 (m), 2962 (m). UV−vis (CH_3CN): 330 nm (sh, 6700 M^{-1} cm^{-1}), 559 (350 M^{-1} cm^{-1}), 990 (55 M^{-1} cm^{-1}).

Preparation of (TBA)$_5$[PW$_{11}$O$_{39}${MnN}], TBA-3. A solution of **TBA-2(N$_3$)** (3 mL, 1.0 mM, 4 equiv of $TBAN_3$ per Mn^{III}) in MeCN was prepared. It was cooled to −30 °C and photolyzed with a Hg/Xe lamp equipped by a 313 nm filter (P = 14.5 mW) for an hour. The completion of the reaction could be checked by UV−vis spectroscopy. To record the IR spectrum, the solution was then precipitated with ether and quickly washed with ethanol to yield **TBA-3** as a brown solid. Solutions of **TBA-3** should be kept at liquid nitrogen temperature. IR (KBr) ν_{max} (cm^{-1}): 391 (s), 518 (m), 596 (w), 709 (w), 811 (vs), 881 (s), 951 (s), 1061 (s), 1023 (vw), 1093 (m), 1381 (w), 1484 (m), 2874 (m), 2937 (m), 2963 (m). UV−vis (CH_3CN): 379 nm (770 M^{-1} cm^{-1}), 449 (800 M^{-1} cm^{-1}), 990 (sh, 48 M^{-1} cm^{-1}). ^{31}P RMN (CD_3CN/CH_3CN) δ = −11.9 ppm.

Instrumentation. IR spectra were recorded from KBr pellets on a Bio-Rad Win-IR FTS 165 FTIR spectrophotometer, and UV−visible spectra were recorded either on a Varian Cary5E spectrophotometer or a Shimadzu UV-2101 spectrophotometer. Photolysis reactions were performed with a Hg/Xe lamp (Hamamatsu, LC6 Lightningcure, 150 W) equipped with filters of appropriate wavelengths. X-band EPR spectra were recorded on a Bruker ESR 300 X-band spectrometer. ^{31}P NMR spectra (121.5 MHz) were obtained at room temperature in 5 mm o.d. tubes on a Bruker AC 300 spectrometer equipped with a QNP probehead. ^{31}P chemical shifts are given with respect to 85% H_3PO_4 (measured by the substitution method) by using $(NBu_4)_3[PW_{12}O_{40}]$ as an internal standard (δ = −14.09 ppm). The ESI mass spectra were recorded by using an ion-trap mass spectrometer (Bruker Esquire 3000, Bremen, Germany) equipped with an orthogonal ESI source operated in the negative ion mode. The capillary high voltage was set to +3500 V. The capillary exit, skimmer 1, and skimmer 2, were typically set to −35, −10, and −6 V, respectively, in order to minimize in-source decomposition. The declustering conditions have been controlled by changing the capillary exit − skimmer 1 potential difference. The ion trap was operated in the standard mode (13 000 m/z/s, 3000 m/z range). Sample solutions (10 pmol μL^{-1} in acetonitrile) were infused into the ESI source by using a syringe pump at a flow rate of 120 μL h^{-1}.

Cyclic voltammetry at a carbon electrode was carried out using the EG&G model 273A system. A standard three-electrode cell was used, which consisted of the working vitrous carbon electrode, an auxiliary platinum electrode, and an aqueous saturated calomel electrode equipped with a double junction. The scan rate was 100 mV/s. Each studied product was dissolved in distilled acetonitrile at a concentration of 10^{-3} M using tetrabutylammonium tetrafluoroborate as an electrolyte (10^{-1} M).

Acknowledgment. The present research was supported by the ANR-06-BLAN-0249-01 grant (fellowship to G.I.).

Supporting Information Available: Low-temperature UV−vis spectrum of **TBA-2(N$_3$)**. EPR spectra of **TBA-1(OH$_2$)** and **TBA-1(N$_3$)**. IR spectra of **TBA-2(OH$_2$)**, **TBA-1(N$_3$)**, **TBA-2(N$_3$)**, and **TBA-3**. ^{31}P NMR spectrum of **TBA-3**. CV of **TBA-2**. UV−vis monitoring of the photolysis of **TBA-2(N$_3$)** at 365 nm, at room temperature and −30 °C. This material is available free of charge via the Internet at http://pubs.acs.org.

(52) Souchay, P. *Polyanions et polycations*; Gauthier-Villars: Paris, 1963.
(53) Pearson, A. J.; Khan, M. N. I.; Clardy, J. C.; Cun-Heng, H. *J. Am. Chem. Soc.* **1985**, *107*, 2748–2757.